IJMMM International Journal of Minerals, Metallurgy and Materials 矿物冶金与材料学报（英文版）

# Preparation and characterization of ceramic materials with low thermal conductivity and high strength using high-calcium fly ash

Mana Rodchom, Panida Wimuktiwan, Kanit Soongprasit, Duangduen Atong, and Supawan Vichaphund

Cite this article as:
Mana Rodchom, Panida Wimuktiwan, Kanit Soongprasit, Duangduen Atong, and Supawan Vichaphund, Preparation and characterization of ceramic materials with low thermal conductivity and high strength using high-calcium fly ash, *Int. J. Miner. Metall. Mater.*, 29(2022), No. 8, pp. 1635-1645. https://doi.org/10.1007/s12613-021-2367-2

View the article online at SpringerLink or IJMMM Webpage.

---

**Articles you may be interested in**

Franco Mayanglambam and Mark Russell, Reusing oxide-based pulverised fly ash and medical waste particles to develop electroless nickel composite coatings (Ni–P/fly ash and Ni–P/$SiO_2$–$Al_2O_3$), *Int. J. Miner. Metall. Mater.*, 27(2020), No. 8, pp. 1147-1156. https://doi.org/10.1007/s12613-020-2071-7

Jia-xin Wen, Tian-bin Zhu, Zhi-peng Xie, Wen-bin Cao, and Wei Liu, A strategy to obtain a high-density and high-strength zirconia ceramic via ceramic injection molding by the modification of oleic acid, *Int. J. Miner. Metall. Mater.*, 24(2017), No. 6, pp. 718-725. https://doi.org/10.1007/s12613-017-1455-9

Xiao-min You, Xue-feng She, Jing-song Wang, Qing-guo Xue, and Ze-yi Jiang, Preparation of CaO-containing carbon pellets from coking coal and calcium oxide: Effects of temperature, pore distribution and carbon structure on compressive strength in pyrolysis furnace, *Int. J. Miner. Metall. Mater.*, 28(2021), No. 7, pp. 1153-1163. https://doi.org/10.1007/s12613-021-2255-9

Shao-chun Chen, Hong-xiang Ye, and Xin-qiang Lin, Effect of rare earth and alloying elements on the thermal conductivity of austenitic medium manganese steel, *Int. J. Miner. Metall. Mater.*, 24(2017), No. 6, pp. 670-674. https://doi.org/10.1007/s12613-017-1449-7

Hao Liu, Nan Wei, Zhou-fu Wang, Xi-tang Wang, and Yan Ma, Fabrication and properties of aluminum silicate fibrous materials with *in situ* synthesized $K_2Ti_6O_{13}$ whiskers, *Int. J. Miner. Metall. Mater.*, 24(2017), No. 11, pp. 1335-1340. https://doi.org/10.1007/s12613-017-1525-z

Hui Xu, Jian-hao Chen, Shu-bin Ren, Xin-bo He, and Xuan-hui Qu, Sintering behavior and thermal conductivity of nickel-coated graphite flake/copper composites fabricated by spark plasma sintering, *Int. J. Miner. Metall. Mater.*, 25(2018), No. 4, pp. 459-471. https://doi.org/10.1007/s12613-018-1592-9

IJMMM WeChat

QQ author group

*International Journal of Minerals, Metallurgy and Materials*
*Volume 29, Number 8, August 2022, Page 1635*
**https://doi.org/10.1007/s12613-021-2367-2**

# Preparation and characterization of ceramic materials with low thermal conductivity and high strength using high-calcium fly ash

*Mana Rodchom, Panida Wimuktiwan, Kanit Soongprasit, Duangduen Atong, and Supawan Vichaphund*✉

Ceramics and Construction Materials Research Group, National Metal and Materials Technology Center (MTEC), National Science and Technology Development Agency (NSTDA), Khlong Nueng, Khlong Luang, Pathumthani 12120, Thailand
(Received: 26 April 2021; revised: 28 September 2021; accepted: 21 October 2021)

**Abstract:** High calcium-fly ash (HCFA) collected from the Mae Moh electricity generating plant in Thailand was utilized as a raw material for ceramic production. The main compositions of HCFA characterized by X-ray fluorescence mainly consisted of 28.55wt% $SiO_2$, 16.06wt% $Al_2O_3$, 23.40wt% CaO, and 17.03wt% $Fe_2O_3$. Due to high proportion of calcareous and ferruginous contents, HCFA was used for replacing the potash feldspar in amounts of 10wt%–40wt%. The influence of substituting high-calcium fly ash (0–40wt%) and sintering temperatures (1000–1200°C) on physical, mechanical, and thermal properties of ceramic-based materials was investigated. The results showed that the incorporation of HCFA in appropriate amounts could enhance the densification and the strength as well as reduce the thermal conductivity of ceramic samples. High proportion of calcareous and ferruginous constituents in fly ash promoted the vitrification behavior of ceramic samples. As a result, the densification was enhanced by liquid phase formation at optimum fly ash content and sintering temperature. In addition, these components also facilitated a more abundant mullite formation and consequently improved flexural strength of the ceramic samples. The optimum ceramic properties were achieved with adding fly ash content between 10wt%–30wt% sintered at 1150–1200°C. At 1200°C, the maximum flexural strength of ceramic-FA samples with adding fly ash 10wt%–30wt% (PSW-FA(10)–(30)) was obtained in the range of 92.25–94.71 MPa when the water absorption reached almost zero (0.03%). In terms of thermal insulation materials, the increase in fly ash addition had a positively effect on the thermal conductivity, due to the higher levels of porosity created by gas evolving from the inorganic decomposition reactions inside the ceramic-FA samples. The addition of 20wt%–40wt% high-calcium fly ash in ceramic samples sintered at 1150°C reduced the thermal conductivity to 14.78%–49.25%, while maintaining acceptable flexural strength values (~45.67–87.62 MPa). Based on these promising mechanical and thermal characteristics, it is feasible to utilize this high-calcium fly ash as an alternative raw material in clay compositions for manufacturing of ceramic tiles.

**Keywords:** ceramic materials; high-calcium fly ash; strength; thermal conductivity

## 1. Introduction

A large amount of coal fly ash (CFA) has been generated from coal-based thermal power plants from several kinds of industries throughout the world every year. It is estimated that the world production of fly ash generated in 2003 was around 430 Mt and will continue to grow in the future [1]. Commonly, these solid wastes are disposed in landfills causing severe environmental problems including water and air pollution, and environmental hazards. Thus, the utilization of fly ash as a value-added product has been widely focused, from the economic viewpoint and solving environmental issues caused by them. Being rich in $SiO_2$ and $Al_2O_3$, as well as a low-cost resource material, fly ash is considered as a suitable candidate for wide usage in several applications, such as soil amendment [2–3], gas adsorbents [4–5], water purification [3], catalyst [6–8], and construction and building materials [9–19]. Among these applications, the utilization of fly ash in the construction and building materials including cement [9–11], geopolymer [12–15], and ceramic materials [16–19], have been put into practice. Besides cement and geopolymer applications, fly ash has been extensively used as an alternative resource and a low-cost raw material for replacing ceramic components such as quartz and potash feldspar to improve the densification as well as reduce the sintering temperature in ceramic tiles [16–19].

Dana *et al.* [16] substituted quartz by 5wt%–15wt% fly ash in a triaxial porcelain composition to enhance the densification and strength of ceramic tiles. The optimum temperature of 1150–1300°C improved the densification with a maximum density of 2.46 g/cm$^3$, while fly ash contributed to enhance the strength up to 70.5 MPa at 1300°C with the sample containing 15wt% fly ash. Mukhopadhyay *et al.* [17] studied the replacement of both quartz and feldspar by fly ash in a porcelain composition to maximize the valorization of fly ash. They reported that the maximum flexural strength of samples was achieved with the addition of 30wt% fly ash, at 72.3 MPa, with the apparent porosity almost being 0. In addi-

✉ Corresponding author: Supawan Vichaphund E-mail: supawank@mtec.or.th
© University of Science and Technology Beijing 2022

tion, Luo *et al.* [18] investigated the steps involving the alkali activation pre-treatment of CFA for preparing fully ash-based ceramic tiles and reported that the fully ash-ceramic product with the alkali treatment showed the superior sintering properties, such as low firing temperature and higher strength of 50 MPa with water absorption value of 0. Wang *et al.* [19] utilized high alumina-fly ash (HAFA) with 30wt%–80wt% for producing ceramic tiles and suggested that the presence of impurities (i.e., CaO and $Fe_2O_3$) in HAFA, which not only narrowed down the densification temperature, but also lessened the bloating temperature of ceramic tiles. At 1300°C, the ceramic sample with 70wt% HAFA demonstrated the highest flexural strength with a relatively apparent porosity of only 0.13%.

However, most of the studies have mainly focused on the use of fly ash with low calcium content (≤10wt%) in ceramic production for enhancing solely the physical-mechanical properties. Thus, to our knowledge, there has been no report involving the utilization of fly ash with high calcium content for preparing ceramic-based tile products in terms of both physical-mechanical and thermal properties. The valorization of fly ash as a partial raw material for ceramic production has positive effect in terms of reducing the need to use natural raw materials, mitigating the accumulation of fly ash residues, minimize environmental impact, and importantly, increase high-value products [18].

Therefore, this work aimed to utilize high-calcium fly ash (HCFA) collected from Mae Moh generating plant of the electricity generating authority of Thailand, which is annually generated ~3 million tons [20], as a raw material for ceramic production. High-calcium fly ash (HCFA) containing high amounts of calcium content, more than 20wt%, was used for replacing the potash feldspar in amounts of 10wt%–40wt%. The green samples are sintered at various temperatures between 1000 and 1200°C. The effect of fly ash substitution on the physical, mechanical, and thermal properties of the fly ash-based ceramic products was investigated.

## 2. Experimental

### 2.1. Raw materials

The main raw materials for ceramic production consisted of kaolin (Amarin Ceramics Co., Ltd., Thailand), ball clay (Compound Clay Co., Ltd., Thailand), potassium feldspar (Amarin Ceramics Co., Ltd., Thailand) as a fluxing agent, and quartz (Cernic International Co., Ltd., Thailand) as a filler. All raw materials had an industrial grain size of less than 45 μm (325 mesh). Coal fly ash (CFA) collected from the Mae Moh electric power generation plant in Lampang (Thailand) was utilized as an additional raw material. The chemical compositions of all raw materials were determined by X-ray fluorescence (XRF; Rigaku ZSX Primus) analysis as demonstrated in Table 1.

### 2.2. Specimen processing

The ceramic compositions were prepared by mixing 50wt% clay (30wt% kaolin and 20wt% ball clay), 10wt% quartz, and 0wt%–40wt% potassium feldspar. Fly ash was used to replace feldspar proportion in different amounts as shown in Table 2. All raw materials were homogeneously mixed by wet ball milling with distilled water for 5 h using an alumina media. Then, the slurry was dried at 100°C for 24 h and ground in a disc grinding mill machine. Subsequently, the mixed powder was then passed through a 60-mesh screen (250 μm) and was hydraulically compacted using an uniaxial pressing to form a bar-shaped specimens (3 mm × 4 mm × 30 mm) at 92 MPa and disc specimens with a diameter of 35 mm at 82 MPa, respectively. The green density of specimens was in the range of 1.75–1.80 g/cm$^3$. After that, the green specimens were sintered in a muffle furnace at different temperatures in the range of 1000–1200°C for 1 h with a heating rate of 5°C/min. The specimens were naturally cooled down to room temperature in the furnace. The sintered specimens were designed as PSW-FA0 for the sample without the addition of fly ash, and PSW-FA(10)–(40) for the samples with

**Table 1. Chemical composition of the raw materials** wt%

| Raw material | $SiO_2$ | $Al_2O_3$ | CaO | $Fe_2O_3$ | $SO_3$ | $K_2O$ | MgO | $Na_2O$ | $TiO_2$ | $P_2O_5$ | MnO | $ZrO_2$ | LOI |
|---|---|---|---|---|---|---|---|---|---|---|---|---|---|
| Kaolin | 47.49 | 35.85 | 0.02 | 1.18 | 0.04 | 1.78 | 0.10 | 0.03 | 0.06 | 0.04 | 0.05 | 0.01 | 12.86 |
| Ball clay | 50.88 | 29.25 | 0.23 | 2.66 | 0.09 | 3.40 | 0.29 | 0.18 | 1.05 | 0.06 | 0.02 | 0.05 | 11.67 |
| Quartz | 99.40 | 0.05 | 0.13 | 0.02 | 0.01 | 0.02 | 0.05 | 0.02 | — | — | — | — | 0.22 |
| K-feldspar | 64.65 | 16.11 | 0.79 | 0.26 | 0.13 | 15.55 | 0.06 | 1.15 | 0.04 | 0.34 | 0.01 | — | 0.53 |
| Coal fly ash | 28.55 | 16.06 | 23.40 | 17.03 | 7.37 | 2.17 | 2.44 | 1.72 | 0.48 | 0.25 | 0.14 | 0.03 | 0.64 |

Note: LOI—Loss on ignition.

**Table 2. Batch composition of ceramic samples**

| No. | Formulation | Raw material composition / wt% | | | | Fly ash addition / wt% |
|---|---|---|---|---|---|---|
| | | Kaolin | Ball clay | Quartz | K-feldspar | |
| 1 | PSW-FA0 | 20 | 30 | 10 | 40 | 0 |
| 2 | PSW-FA10 | 20 | 30 | 10 | 30 | 10 |
| 3 | PSW-FA20 | 20 | 30 | 10 | 20 | 20 |
| 4 | PSW-FA30 | 20 | 30 | 10 | 10 | 30 |
| 5 | PSW-FA40 | 20 | 30 | 10 | 0 | 40 |

the addition of fly ash (10wt%–40wt%). A flow chart of the experimental procedure is shown in Fig. 1.

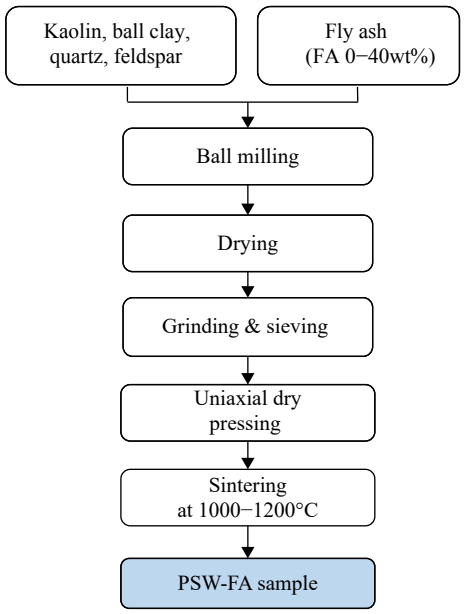


**Fig. 1. Schematic diagram of experimental procedure.**

### 2.3. Characterization

The chemical composition of the raw materials was determined by X-ray fluorescence spectroscopy (XRF; Rigaku ZSX Primus). The particle size and distribution of the fly ash particles were measured using laser diffraction by Mastersizer 2000 (Version 5.54 Serial Number: MAL 1021434, Malvern Instrument Ltd.). The crystalline phases of raw materials and prepared ceramic samples were performed by X-ray diffraction (XRD; PANalytical X'pert pro and XRD; Bruker, D8 ADVANCE, 40 kV and 30 mA, Cu-$K_\alpha$ radiation). The sample was scanned in a diffraction angle range from 10° to 90° with a step size of 0.04. The weight percentage of crystalline phases in each sample was quantitatively analyzed using DIFFRAC.EVA software (version 5.0).

The physical properties including the bulk density, water absorption, and open porosity of the sintered samples were determined by the Archimedes method using distilled water as the liquid media. The linear shrinkage was achieved by measuring the length of samples before and after the sintering process. The three-point bending strength at room temperature was measured with a span of 20 mm and a crosshead speed of 0.5 mm/min (Instron model UTM 8872). The microstructure of the polished surfaces was characterized by using a scanning electron microscope (SEM; HITACHI, SU5000). Energy dispersive X-ray spectroscope (EDS; HORIBA, X-Max) was used for the elemental analysis of chemically etched surfaces. Thermal conductivity measurement was performed on the disk shape (35 mm in diameter and 5 mm in thickness) at the room temperature using a thermal conductivity analyzer (TPS2500S, Hot Disk).

## 3. Results and discussion

### 3.1. Characterization of fly ash and other raw materials

The major chemical components of fly ash were silicon dioxide ($SiO_2$), aluminum oxide ($Al_2O_3$), calcium oxide (CaO), and ferric oxide ($Fe_2O_3$), along with a small amount of magnesium oxide (MgO), potassium oxide ($K_2O$), titanium oxide ($TiO_2$), sodium oxide ($Na_2O$), sulfur trioxide ($SO_3$), and phosphorus pentoxide ($P_2O_5$) as exhibited in Table 1. High amount of CaO (23.40wt%) might have resulted from the lime slurry injected during the air pollution control procedure [21]. Additionally, due to the high content of calcium oxide (more than 20wt%), this fly ash was classified as class C according to ASTM C618 [1]. The XRD result showed that the main mineral phases of fly ash included quartz ($SiO_2$), anhydrite ($CaSO_4$), magnetite ($Fe_3O_4$), and calcium iron oxide ($CaFeO_2$), respectively (Fig. 2(a)). The morphology of fly ash consisted of spherical particles with a median diameter of 29.01 μm as demonstrated in Fig. 2(b) and (c).

The chemical compositions and crystallinity phases of other raw materials are shown in Table 1 and Fig. 3. Kaolin and ball clay mainly consisted of $SiO_2$ and $Al_2O_3$ with a small amount of CaO, MgO, $Fe_2O_3$, $K_2O$, etc. From the XRD results, kaolinite and quartz were found as the main phases in clay materials. These clays contributed to plasticity during the formation of the green body. In addition, the quartz is more than 97% pure silica, which is commonly applied as a filler to reduce distortion and shrinkage in the ceramic materials. Meanwhile, K-feldspar as a fluxing agent involving lowered the liquid formation temperature, mainly composed of $SiO_2$, $Al_2O_3$, and $K_2O$ [18]. Being rich in $SiO_2$, $Al_2O_3$, and CaO, fly ash can be utilized as an additional raw material (a feldspar substitute) for ceramic tile production.

### 3.2. Post-sintering properties of sintered samples

3.2.1. Physical and mechanical properties

The sintered color of samples with different additions of

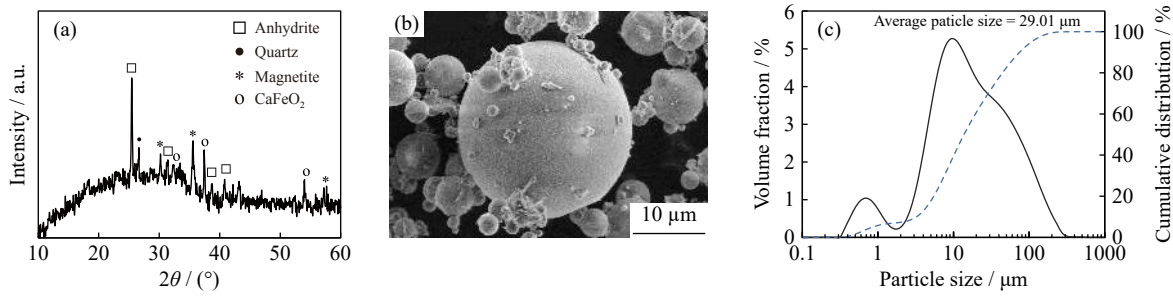


**Fig. 2. Fly ash characterization: (a) XRD pattern, (b) SEM micrograph, and (c) particle size distribution.**

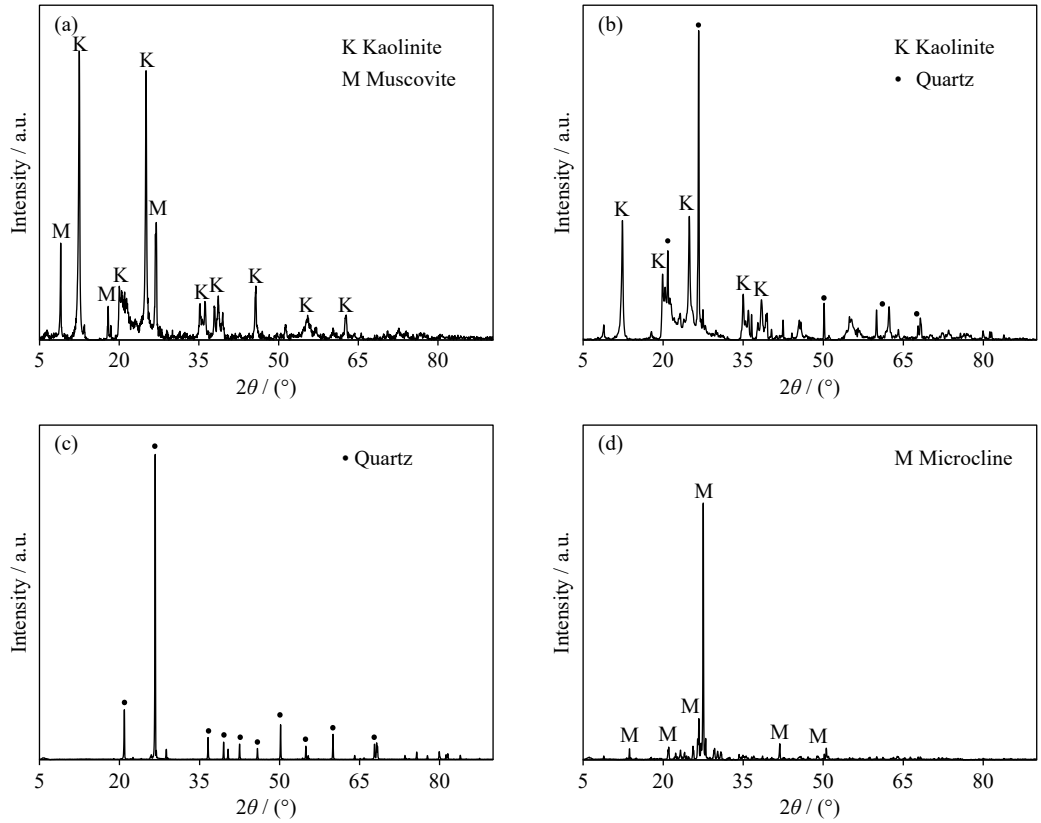


**Fig. 3. XRD patterns of raw materials: (a) kaolin, (b) ball clay, (c) quartz, and (d) K-feldspar.**

fly ash sintered at 1000–1200°C is observed by the naked eye as displayed in Fig. 4. Colors of the ceramic-fly ash samples changed on increasing the high calcium fly ash content and sintering temperature. The ceramic samples without fly ash addition (PSW-FA0) changed to a brown color after sintering at 1200°C. Whereas, the increasing fly ash content in ceramic body resulted in a more reddish-brown color and became dark for the sample of PSW-FA sintered at a higher temperature. This was due to the increase of $Fe_2O_3$ content in the ceramic matrix [22–23].

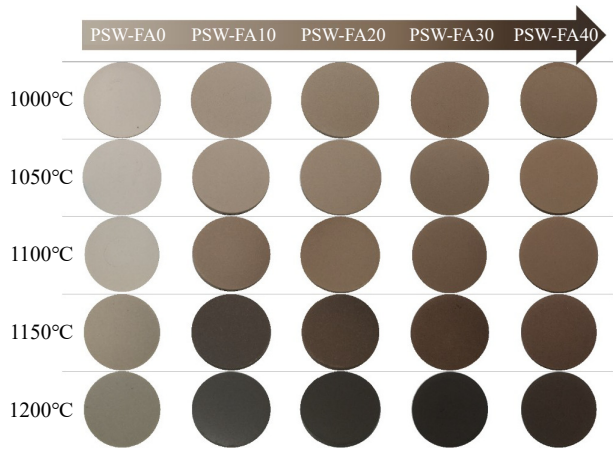


**Fig. 4. Color changing of ceramic-(0–40wt%)FA samples at different temperatures from 1000 to 1200°C.**

In this study, the ceramic-(0–40wt%)FA samples were successfully prepared at the temperature range of 1000–1200°C. The influence on physical properties of sintering temperature and the replacement of K-feldspar with high-calcium fly ash (0–40wt%) were investigated. The linear shrinkage, bulk density, open porosity, and water absorption are shown in Fig. 5(a)–(d). Fig. 5(a) illustrates the linear shrinkage of ceramic-fly ash samples as a function of sintering temperature. The maximum value of linear shrinkage was 7.6%–11.9% obtained at 1200°C. It can be observed that the linear shrinkage of samples was significantly affected due to the replacement of feldspar by fly ash. The addition of fly ash in high content (20wt%–40wt%) decreased the shrinkage considerably at temperature up to 1150°C. This expansion might be due to the decomposition of $CaSO_4$ from fly ash compositions at high temperatures which generates sulfur dioxide gas ($SO_2$) as shown in Eq. (1) [19,24]. Therefore, $CaSO_4$ compounds cannot detected in the PSW-FA specimens at high sintering temperature as shown in the XRD results (section 3.2.2). In this case, $CaSO_4$ contained in fly ash acted as a foaming agent to produce the coalescent pores inside ceramic bodies during sintering process. Additionally, another possible reason of this expansion could be resulted from either the expansion of $O_2$ generated from the transformation of $Fe_2O_3$ to $Fe_3O_4$ or the expansion of gas entrapped into the close pore at high temperature (~1200°C) [17,19,25–26].

$$CaSO_4 \xrightarrow{\sim 1100-1200^{\circ}C} CaO + SO_2 \uparrow + 0.5O_2 \uparrow \quad (1)$$

The evolution of the bulk density with sintering temperature ceramic-fly ash samples is displayed in Fig. 5(b). The results indicated that the densification of ceramic-FA samples increased significantly with raised sintering temper-

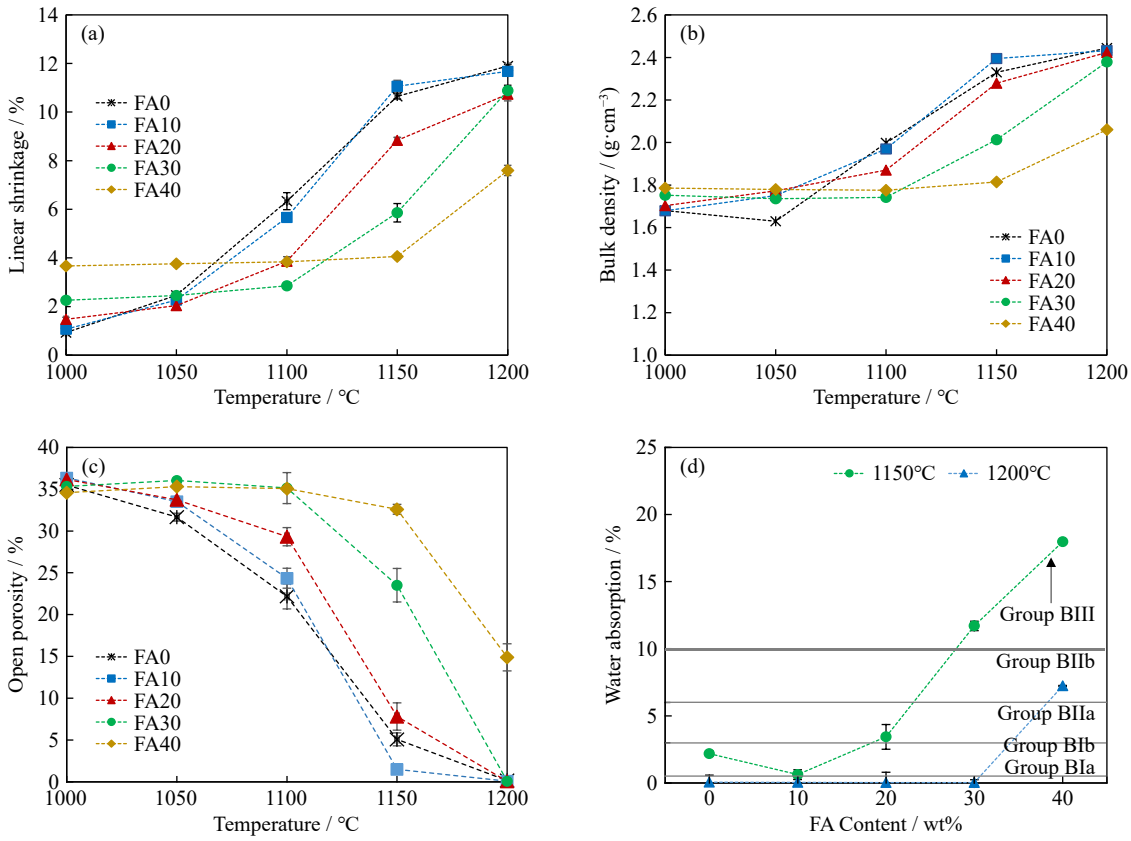


**Fig. 5. Physical properties of ceramic-(0–40wt% FA)samples at different temperatures: (a) linear shrinkage, (b) bulk density, (c) open porosity, and (d) water absorption.**

atures, and reached a maximum value of 2.06–2.44 g/cm$^3$ at 1200°C. It can be noted that the increase of sintering temperature contributed to accelerating the further generation of the liquid phase, which can fill the pore, leading to a reduction of porosity in the samples and promotion of densification [24,27]. The bulk density reached to 2.38–2.43 g/cm$^3$ at 1200°C as the fly ash content increased to 10wt%–30wt% (PSW-FA10, PSW-FA20, and PSW-FA30), which is consistent with that of the reference samples (PSW-FA0, 2.44 g/cm$^3$) and dense porcelain tiles (2.3–2.5 g/cm$^3$) [28–29]. It indicated that the appropriate amount of high calcium-fly ash, with the presence of calcium oxide and ferric oxide, improved the densification of samples. According to the liquid formation during the sintering process, these alkaline metal oxides in fly ash enhanced the generation of low melting liquid phase, leading to the improvement of densification of samples [24]. However, the addition of higher fly ash (40wt%) influenced significantly in the decrease of bulk density at temperature range of 1100–1200°C. This may be due to the higher level of porosity generating from the gas evolving inside the ceramic-FA samples, which corresponds to the open porosity values.

Fig. 5(c) shows the open porosity of ceramic-fly ash samples as a function of temperature, where the porosity of the ceramic-FA samples decreased as the sintering temperature increased. The open porosity drastically decreased after sintering at 1100°C for all samples. The lowest porosity was 0.06%–0.08% for PSW-FA(10)–(30) sintered at 1200°C. The result indicated that the substitution of fly ash containing CaO in an appropriate amount improved the densification degree of ceramic-FA products by increasing the viscous flow into the inter-granular pores at high temperature. Consequently, the smaller pore size or/and lower porosity were obtained. This result corresponded with the findings of a previous work reported by Hossian *et al.* [23], who investigated the replacement of K-feldspar by silt and wollastonite and found that the apparent porosity reduced significantly to 0.45% when adding 20wt% silt and 30wt% wollastonite at 1130°C. They suggested that a high quantity of CaO in a wollastonite composition aided the densification by improving viscous flow. As a result, the pore size considerably shrank and the packing of samples effectively increased leading to higher density and lower porosity.

In terms of the water absorption as shown Fig. 5(d), these values were less than 5% for PSW-FA(0)–(20) samples sintered at 1150°C. At a higher temperature of 1200°C, the water absorption of PSW-FA(10)–(30) continuously dropped to 0.03%, which is lower than the ISO 13006 standards (≤ 0.5wt%) [30]. Whereas the clay-based product (PSW-FA0) showed a slightly higher water adsorption value of 0.06%. Unfortunately, the addition of fly ash up to 40wt% (PSW-FA40) resulted in the increase of water absorption at 7.23% at a high temperature (1200°C). This result indicated that the excessive alkali metal oxide in fly ash and the heat treatment of ceramic-FA samples caused an overfiring effect [17,29]. This phenomenon resulted from high proportion of alkaline earth oxide (i.e., CaO, $K_2O$) and ferruginous oxide constituents found in ceramic mixtures containing high content of fly

ash. Generally, these components promoted the vitrification behavior of ceramic samples. In case of CaO component, it acted as a modifier of slilicate networks. The $Ca^{2+}$ ions can diffuse into the liquid phase and therefore, promote the depolymerization of silicate networks leading to lowering the viscosity of the liquid phase [25,31]. As a result, the densification was enhanced by liquid phase formation at optimum fly ash content and sintering temperature. However, the excessive fluxing agents with high temperature beyond vitrification (apparent porosity < 0.5%), the open pore of ceramic samples became to zero, whilst the close porosity increased considerably leading to bloating. The reason of bloating may come from the expansion of gases trapped inside the close pores at high temperature. In this work, therefore, the increase of water absorption rate resulted from more porosity generating inside the ceramic body can be observed for PSW-FA40 sample, which is consistent with the increase in the open porosity as shown in Fig. 5(c) [17,26].

The flexural strength of ceramic-(0–40wt%)FA specimens sintered at 1000–1200°C is displayed in Fig. 6. The flexural strength of ceramic-(0–40wt%) FA specimens was a function of the sintering temperature. At 1150°C, the flexural strength of ceramic containing fly ash (10wt%–20wt%) was higher (70.92–87.62 MPa) than that of the ceramic sample (PSW-FA0, 67.36 MPa). This result agreed well with the findings of Dana *et al.* [16], who studied the influence of fly ash on porcelain composition by replacing quartz. They reported that the strength of 5wt%–15wt% fly ash containing samples (35–65 MPa) was found to be greater than that of the reference batch (25–45 MPa) at high temperature, 1150–1250°C. They also suggested that the higher strength resulted from the formation of a large amount of low silica glass in the presence of fluxing components including CaO, $Fe_2O_3$, $K_2O$, and $Na_2O$ facilitating a more abundant mullite formation. It was also confirmed that the fly ash addition with high CaO content contributed to promote a more effective densification of the ceramic samples, and consequently a higher flexural strength was obtained [32]. When increasing temperature up to 1200°C, the maximum flexural strength of ceramic-FA samples with adding fly ash 10wt%–30wt% was obtained in the range of 92.25–94.71 MPa. Based on ISO 13006 (1998), ceramic-(10wt%–40wt%)FA samples sintered at 1150–1200°C can be classified as an absorption group B (pressed), because their water absorption and strength values fitted into this classification, as shown in Table 3.

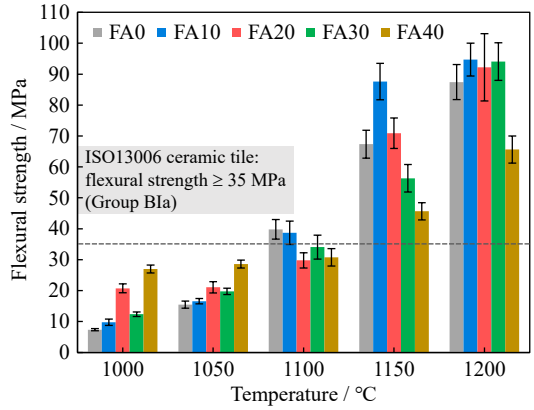


**Fig. 6. Flexural strength of ceramic-FA specimens.**

**Table 3. Classification and properties of ceramic-FA samples**

| No. | Samples | Fly ash / wt% | Sintering temperature / °C | Water adsorption / % | Flexural strength / MPa |
|---|---|---|---|---|---|
| Group BIa | PSW-FA10 | 10 | 1200 | 0.03 | 94.71 |
| | PSW-FA20 | 20 | 1200 | 0.03 | 92.25 |
| | PSW-FA30 | 30 | 1200 | 0.03 | 94.07 |
| Group BIb | PSW-FA10 | 10 | 1150 | 0.62 | 87.62 |
| Group BIIa | PSW-FA20 | 20 | 1150 | 3.43 | 70.92 |
| Group BIIb | PSW-FA40 | 40 | 1200 | 7.23 | 65.63 |
| Group BIII | PSW-FA30 | 30 | 1150 | 11.70 | 56.33 |
| | PSW-FA40 | 40 | 1150 | 17.97 | 45.67 |

3.2.2. Phase analysis and microstructure

Phase compositions and microstructure characteristics of samples are considered as important parameters involving both physical and mechanical properties. The influence of sintering temperature on the difference of phase compositions of ceramic containing fly ash specimens is exhibited in Table 4 and Fig. 7(a). At lower temperature (1000–1050°C), the crystalline phases of fly ash derived ceramic samples were mainly quartz ($SiO_2$, JCPDS: 00-046-1045) and anorthite ($CaAl_2Si_2O_8$, JCPDS: 00-041-1481) with small amount of calcium sulphate (anhydrite ($CaSO_4$), JCPDS: 00-037-1496). With increasing the sintering temperature (1100–1200°C), the quartz phase decreased significantly, while the intensity of anorthite increased gradually. The mullite content ($3Al_2O_3{\cdot}2SiO_2$, JCPDS: 00-019-0776) increased with the temperature for the samples with fly ash content of (10–30)wt%, while the reduction of mullite content was observed at the sample containing high fly ash content of 40wt% (PSW-FA40). As illustrated in Table 4 and Fig. 7(a), the calcium sulphate disappeared at the temperature above 1050°C, due to the $CaSO_4$ decomposition leading to the expansion of gas entrapped into the close pore at high temperature as mentioned in section 3.2.1.

Fig. 7(b) shows the X-ray diffraction patterns of the samples with different fly ash addition (0–40wt%) sintered at 1200°C. It was found that the crystalline phases of the fly

**Table 4. Phase analysis of selected PSW-FA samples sintered at 1000–1200°C**

| Sample | Temperature / °C | Crystallinity / wt% | | | | Amorphous / wt% |
|---|---|---|---|---|---|---|
| | | Quartz | Anorthite | Anhydrite | Mullite | |
| PSW-FA10 | 1000 | 41.0 | 8.4 | 2.2 | — | 48.4 |
| | 1050 | 41.5 | 11.8 | 0.7 | — | 45.9 |
| | 1100 | 31.8 | 10.7 | — | 7.8 | 49.8 |
| | 1150 | 28.6 | 11.6 | — | 9.0 | 50.7 |
| | 1200 | 28.4 | 9.4 | — | 12.8 | 49.3 |
| PSW-FA20 | 1000 | 31.3 | 26.7 | 1.9 | — | 40.2 |
| | 1050 | 25.4 | 28.2 | 2.2 | — | 44.2 |
| | 1100 | 19.9 | 31.4 | — | 6.4 | 42.2 |
| | 1150 | 9.1 | 39.4 | — | 5.0 | 46.5 |
| | 1200 | 6.6 | 30.1 | — | 12.0 | 51.3 |
| PSW-FA30 | 1000 | 33.2 | 13.9 | 2.7 | — | 50.2 |
| | 1050 | 33.9 | 13.5 | 2.0 | — | 50.6 |
| | 1100 | 24.8 | 24.9 | — | 8.2 | 42.1 |
| | 1150 | 14.8 | 32.9 | — | 8.7 | 43.7 |
| | 1200 | 13.3 | 26.5 | — | 11.8 | 48.4 |
| PSW-FA40 | 1000 | 27.9 | 23.6 | 7.1 | — | 46.5 |
| | 1050 | 21.7 | 34.6 | 1.5 | — | 42.2 |
| | 1100 | 16.0 | 34.8 | — | 5.5 | 43.7 |
| | 1150 | 9.0 | 43.7 | — | 3.4 | 44.0 |
| | 1200 | 3.2 | 50.9 | — | 4.5 | 41.4 |

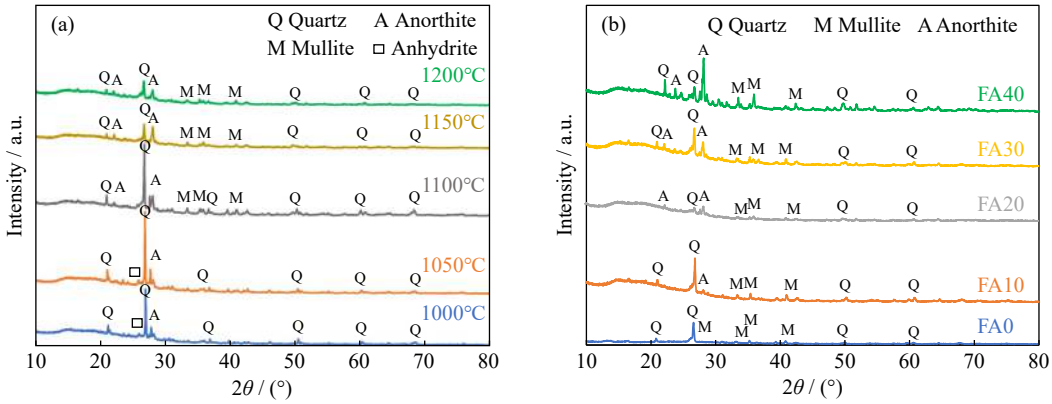


**Fig. 7. XRD patterns of samples: (a) PSW-30FA samples sintered at 1000–1200°C and (b) PSW-FA samples with different fly ash contents (0–40wt%) sintered at 1200°C.**

ash-free ceramic samples (PSW-FA0) consisted of quartz ($SiO_2$, JCPDS: 00-046-1045) and mullite ($3Al_2O_3{\cdot}2SiO_2$, JCPDS: 00-019-0776), which was generally found at a higher sintering temperature (1200–1300°C). The formation of mullite led to the improvement of densification and strength of samples. Meanwhile, the crystalline phases detected in the ceramic-(10wt%–40wt%)FA samples were anorthite ($CaAl_2Si_2O_8$, JCPDS: 00-041-1481), quartz, and mullite. The formation of anorthite might be due to the reaction between metakaolinite ($Al_2O_3{\cdot}2SiO_2$) in the clay composition with CaO species in the fly ash, according to Eq. (2) [32].

$$3Al_2O_3 \cdot 2SiO_2 + 4SiO_2 + 3CaO \rightarrow 3\,[CaO \cdot Al_2O_3 \cdot 2SiO_2] \quad (2)$$

As a result, the incorporation of fly ash 40wt% resulted in the reduction of quartz and consequently, the formation of anorthite increased significantly. Moreover, the higher proportion of mullite was observed because of the high amount of alkaline and alkaline earth oxide in fly ash (i.e., CaO, $K_2O$, $Na_2O$, and MgO) facilitating the crystallization of mullite [33–34].

Fig. 8 shows the SEM micrographs of samples with different fly ash contents in the range of 0–40wt% sintered at 1200°C. The SEM examination confirmed the change in porosity of sintered ceramic samples was due to addition of fly ash. A denser structure and a uniform micro-pore distribution were distinctly observed in the sample PSW-FA0. The increase of fly ash content in the range of 10wt%–30wt% promoted a high quantity of liquid phase during the sintering process, which can easily fill up the open pores [16,33]. Therefore, the samples with 10wt%–30wt% had a sintered

microstructure and appeared as isolated pores with a size of 5–20 μm. However, the higher proportion of porosity was found on the fracture surface of the ceramic sample with 40wt% fly ash. This porosity may be due to the evolution of gas from the inorganic decomposition reactions inside the ceramic-FA samples. This high porosity was consistent with the increase in water absorption and the decrease in strength as mentioned above (section 3.2.1). In addition, Fig. 9 exhibits well-formed needle-shaped secondary mullite forming a network distributed throughout the sample PSW-FA10 and PSW-FA30 [34]. SEM–EDS analysis indicated that the elements of needle-like mullite crystals mainly consisted of Si and Al with small amounts of fluxing elements such as Ca, Fe, and K.

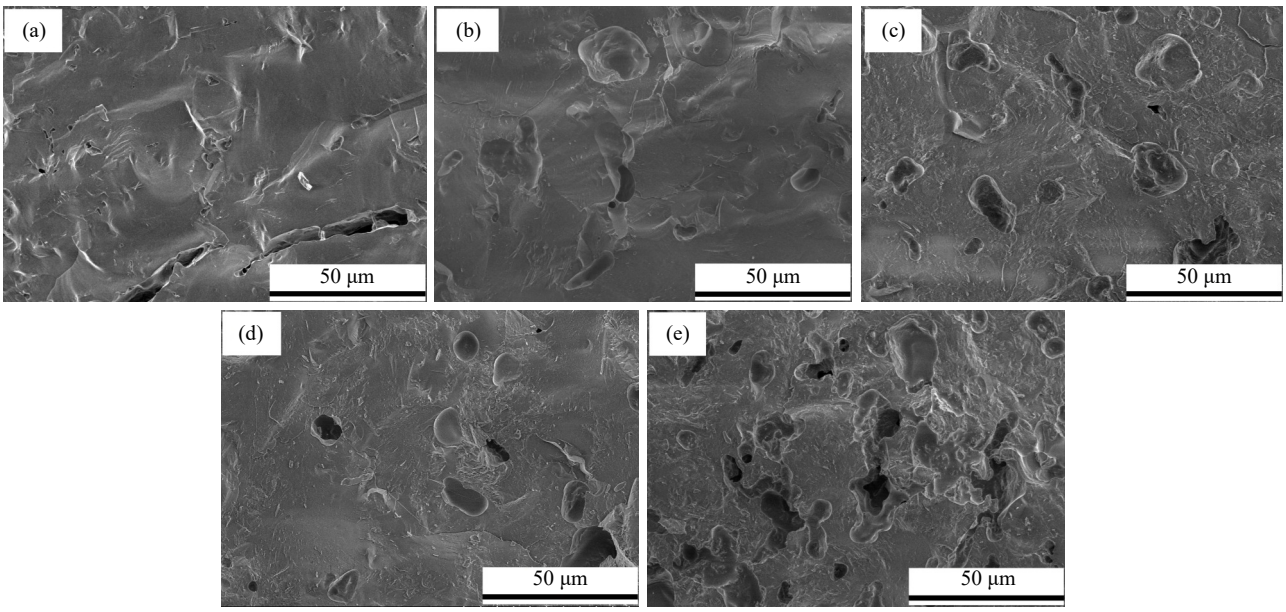


**Fig. 8. SEM micrographs of the ceramic-(0–40wt%)FA samples after sintered at 1200°C: (a) PSW-FA0, (b) PSW-FA10, (c) PSW-FA20, (d) PSW-FA30, and (e) PSW-FA40.**

During sintering process, high proportion of alkaline earth oxides (i.e., CaO, $Na_2O$, $K_2O$) in fly ash can function as a modifier of slilicate networks to decrease the viscosity of the liquid phase leading to the increase in the mass transfer rate. Meanwhile, the presence of $Fe^{3+}$ promoted the formation of mullite from the glassy phase by replacing $Al^{3+}$ in its structure [16–17]. Thus, the primary mullite can be initially formed at temperature around 1100°C [35], while the growth of secondary mullite can be described on the enhanced formation and lower melting point of glassy phase, allowing dissolution–reprecipitation in the glass at lower sintering temperature ~1200°C [36–37]. The formation of the needle-shaped mullite at the lower temperature (1200°C) has been reported by Dana *et al.* [16], who confirmed that mullite formation can be observed at the low temperature (1150–1200°C) for ceramic containing fly ash (5wt%–10wt%). Additionally, ceramic containing fly ash bodies with lower quartz content and higher alkaline species (i.e., CaO, $Fe_2O_3$, $Na_2O$). Meanwhile, Mukhopadhyay *et al.* [17] suggested that the formation of needle-shaped secondary mullite can be found throughout the ceramic-(25wt%–30wt%)FA samples sintered at the temperature of 1250°C. The interlocking and uniform distribution of these secondary mullite needles in the glassy matrix contributed to promoting the flexural strength. Thus, these high levels of mullite crystals in the matrix contributed toward the development of the flexural strength remarkably, reaching a maximum value of 94.07–94.71 MPa at 1200°C.

3.2.3. Thermal property

Fig. 10 shows the effect of fly ash content in the range 0–40wt% and sintering temperature (1000–1200°C) on thermal conductivity. The thermal conductivity of the fly ash containing ceramic samples is strongly influenced by the firing temperature. A rise of the sintering temperature increased the thermal conductivity of the ceramic-FA samples. Zhang *et al.* [38] suggested that the high temperature could reduce the level of porosity inside the sample and then improve the densification, which directly affect the thermal conductivity. As a result, the thermal conductivity of samples with 10wt%–40wt% fly ash contents at 1150°C, 0.66–1.25 $W \cdot m^{-1} \cdot K^{-1}$ showed quite lower values compared to that of samples with 10wt%–40wt% fly ash contents at 1200°C, 0.86–1.28 $W \cdot m^{-1} \cdot K^{-1}$. Meanwhile, the thermal conductivity significantly decreased with the increase in fly ash addition, due to the higher levels of porosity created by gas evolving from the inorganic decomposition reactions inside the ceramic-FA samples. In terms of thermal insulation materials, the addition of 20wt%–40wt% high-calcium fly ash in the ceramic samples sintered at 1150°C reduced the thermal conductivity to 14.78%–49.25%, while maintaining superior flexural strength values (~45.67–87.62 MPa) as shown in Fig. 11. Based on these promising mechanical and thermal characteristics, it is feasible to utilize high-calcium fly ash as

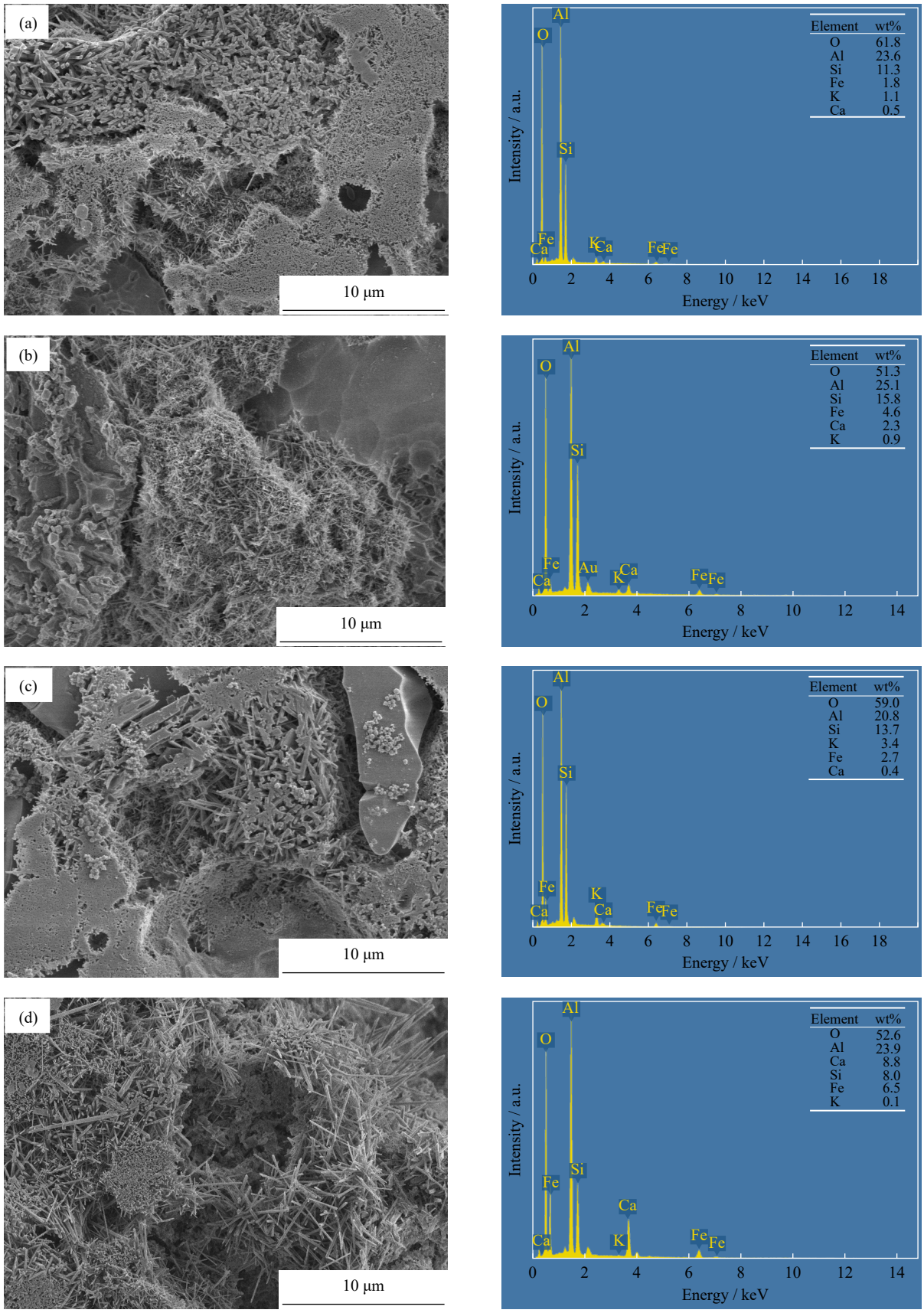


**Fig. 9. SEM micrographs and EDS analysis of the ceramic-FA samples sintered at 1200°C: (a) PSW-FA10, (b) PSW-FA20, (c) PSW-FA30, and (d) PSW-FA40.**

an alternative and a low-cost raw material in clay compositions for ceramic tiles manufacturing and preventing environmental impact associated with the disposal of high-calcium fly ash.

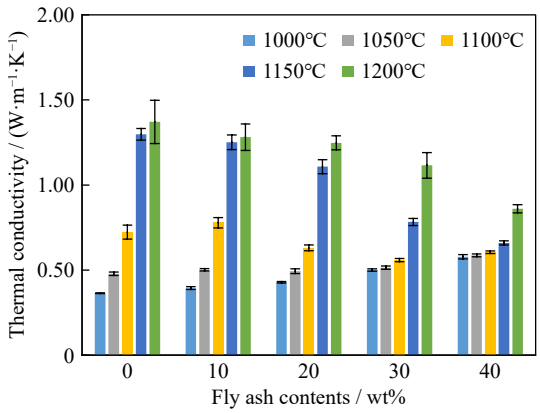


**Fig. 10. Thermal conductivity of the ceramic-(0–40wt%)FA samples after sintered at 1000–1200°C.**

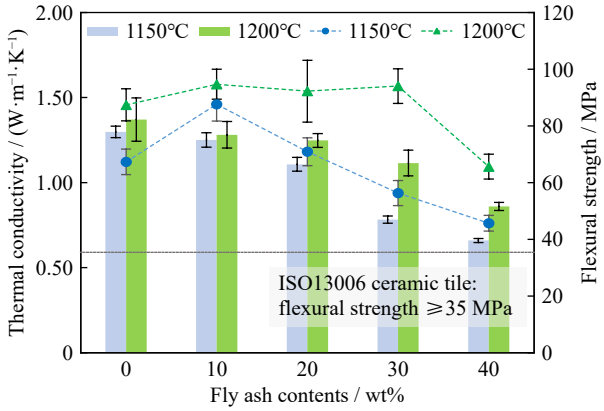


**Fig. 11. Thermal conductivity and strength of the ceramic-(0–40wt%)FA samples after sintered at 1150–1200°C.**

## 4. Conclusion

Ceramic samples containing fly ash were successfully prepared by adding high calcium fly ash in the proportion of 10wt%–40wt% sintered at 1000–1200°C. The replacement of K-feldspar with high-calcium fly ash (10wt%–40wt%) influenced the physical, mechanical, and thermal properties of the clay-based ceramic compositions. The incorporation of fly ash in appropriate amounts could enhance the densification and the strength of samples. The presence of fluxing components in fly ash, particularly CaO and $Fe_2O_3$, facilitating a more abundant mullite formation and consequently improving flexural strength of ceramic samples. The samples with 10wt%–40wt% fly ash sintered at 1150–1200°C could fulfill the ISO standard and offered high flexural strength in the range of 45.67–94.71 MPa. The optimum ceramic properties were achieved with adding fly ash content between 10wt%–30wt% sintered at 1150–1200°C. At 1200°C, the maximum flexural strength of ceramic-FA samples with adding fly ash 10wt%–30wt% was obtained in the range of 92.25–94.71 MPa, when the water absorption had almost reached zero (0.03%). In terms of the property of thermal conductivity, the addition of 20wt%–40wt% high-calcium fly ash in ceramic samples sintered at 1150°C reduced the thermal conductivity to 14.78%–49.25%, while maintaining an acceptable flexural strength values (~45.67–87.62 MPa). Based on these superior mechanical and thermal characteristics, it is feasible to utilize high-calcium fly ash as an alternative raw material in clay compositions for ceramic tiles manufacturing and preventing environmental impacts associated with the disposal of high-calcium fly ash.

## Acknowledgement

This work was financially supported by the National Metal and Materials Technology Center, Thailand (Project No. P-18-50327).

## Conflict of Interest

The authors declare no potential conflicts of interest.

## References

[1] S.B. Wang, Application of solid ash based catalysts in heterogeneous catalysis, *Environ. Sci. Technol.*, 42(2008), No. 19, p. 7055.

[2] M. Park, C.L. Choi, W.T. Lim, M.C. Kim, J. Choi, and N.H. Heo, Molten-salt method for the synthesis of zeolitic materials: I. Zeolite formation in alkaline molten-salt system, *Microporous Mesoporous Mater.*, 37(2000), No. 1-2, p. 81.

[3] N. Murayama, H. Yamamoto, and J. Shibata, Mechanism of zeolite synthesis from coal fly ash by alkali hydrothermal reaction, *Int. J. Miner. Process.*, 64(2002), No. 1, p. 1.

[4] J.T. Soe, S.S. Kim, Y.R. Lee, J.W. Ahn, and W.S. Ahn, $CO_2$ capture and $Ca^{2+}$ exchange using zeolite A and 13X prepared from power plant fly ash, *Bull. Korean Chem. Soc.*, 37(2016), No. 4, p. 490.

[5] R. Panek, M. Wdowin, W. Franus, *et al.*, Fly ash-derived MCM-41 as a low-cost silica support for polyethyleneimine in post-combustion $CO_2$ capture, *J. $CO_2$ Util.*, 22(2017), p. 81.

[6] P. Kumar, N. Mal, Y. Oumi, K. Yamana, and T. Sano, Mesoporous materials prepared using coal fly ash as the silicon and aluminium source, *J. Mater. Chem.*, 11(2001), No. 12, p. 3285.

[7] S. Vichaphund, D. Aht-Ong, V. Sricharoenchaikul, and D. Atong, Characteristic of fly ash derived-zeolite and its catalytic performance for fast pyrolysis of Jatropha waste, *Environ. Technol.*, 35(2014), No. 17, p. 2254.

[8] S. Vichaphund, V. Sricharoenchaikul, and D. Atong, Utilization of fly ash-derived HZSM-5: Catalytic pyrolysis of Jatropha wastes in a fixed-bed reactor, *Environ. Technol.*, 38(2017), No. 13-14, p. 1660.

[9] J.J. Feng, J.W. Sun, and P.Y. Yan, The influence of ground fly ash on cement hydration and mechanical property of mortar, *Adv. Civ. Eng.*, 2018(2018), art. No. 4023178.

[10] R. Rajamma, R.J. Ball, L.A.C. Tarelho, G.C. Allen, J.A. Labrincha, and V.M. Ferreira, Characterisation and use of biomass fly ash in cement-based materials, *J. Hazard. Mater.*, 172(2009), No. 2-3, p. 1049.

[11] T.H.M. Le, D.W. Park, J.Y. Park, and T.M. Phan, Evaluation of the effect of fly ash and slag on the properties of cement asphalt mortar, *Adv. Mater. Sci. Eng.*, 2019(2019), art. No. 1829328.

[12] F. Skvara, T. Jilek, and L. Kopecky, Geopolymer materials based on fly ash, *Ceram. Silik.*, 49(2005), No. 3, p. 195.

[13] R.M. Novais, L.H. Buruberri, G. Ascensão, M.P. Seabra, and J.A. Labrincha, Porous biomass fly ash-based geopolymers with tailored thermal conductivity, *J. Clean. Prod.*, 119(2016), p. 99.

[14] S. Alehyen, M.E.L. Achouri, and M. Taibi, Characterization, microstructure and properties of fly ash-based geopolymer, *J. Mater. Environ. Sci.*, 8(2017), No. 5, p. 1783.
[15] J.J. Feng, R.F. Zhang, L.L. Gong, Y. Li, W. Cao, and X.D. Cheng, Development of porous fly ash-based geopolymer with low thermal conductivity, *Mater. Des.*, 65(2015), p. 529.
[16] K. Dana, S. Das, and S.K. Das, Effect of substitution of fly ash for quartz in triaxial kaolin–quartz–feldspar system, *J. Eur. Ceram. Soc.*, 24(2004), No. 10-11, p. 3169.
[17] T.K. Mukhopadhyay, S. Ghosh, J. Ghosh, S. Ghatak, and H.S. Maiti, Effect of fly ash on the physico-chemical and mechanical properties of a porcelain composition, *Ceram. Int.*, 36(2010), No. 3, p. 1055.
[18] Y. Luo, S.L. Zheng, S.H. Ma, C.L. Liu, and X.H. Wang, Ceramic tiles derived from coal fly ash: Preparation and mechanical characterization, *Ceram. Int.*, 43(2017), No. 15, p. 11953.
[19] H. Wang, M.G. Zhu, Y.Q. Sun, R. Ji, L.L. Liu, and X.D. Wang, Synthesis of a ceramic tile base based on high-alumina fly ash, *Constr. Build. Mater.*, 155(2017), p. 930.
[20] EGAT Biznews, *Coal Combustion Products*, Electricity Generating Authority of Thailand (EGAT), Thailand [2020-12-30]. https://www.egatbusiness.com/archive/biznews/2560/BizNews2017-4.pdf
[21] Y. Deng, B. Gong, Y. Chao, *et al*., Sustainable utilization of municipal solid waste incineration fly ash for ceramic bricks with eco-friendly biosafety, *Mater. Today Sustain.*, 1-2(2018), p. 32.
[22] N.U. Kockal, Utilisation of different types of coal fly ash in the production of ceramic tiles, *Bol. Soc. Esp. Ceram. Vidrio*, 51(2012), No. 5, p. 297.
[23] S.S. Hossain, V. Ranjan, R. Pyare, and P.K. Roy, Study the effect of physico-mechanical characteristics of ceramic tiles after addition of river silts and wollastonite derived from wastes, *Constr. Build. Mater.*, 209(2019), p. 315.
[24] H. Wang, Y.Q. Sun, L.L. Liu, R. Ji, and X.D. Wang, Integrated utilization of fly ash and waste glass for synthesis of foam/dense bi-layered insulation ceramic tile, *Energy Build.*, 168(2018), p. 67.
[25] M.K. Zhou, X.X. Ge, H.D. Wang, L.S. Chen, and X. Chen, Effect of the CaO content and decomposition of calcium-containing minerals on properties and microstructure of ceramic foams from fly ash, *Ceram. Int.*, 43(2017), No. 12, p. 9451.
[26] Y. Luo, J.Y. Wang, Y.H. Wu, X.Y. Li, P.K. Chu, and T. Qi, Substitution of quartz and clay with fly ash in the production of architectural ceramics: A mechanistic study, *Ceram. Int.*, 47(2021), No. 9, p. 12514.
[27] R.Y. Chen, Y.B. Li, R.F. Xiang, and S.J. Li, Effect of particle size of fly ash on the properties of lightweight insulation materials, *Constr. Build. Mater.*, 123(2016), p. 120.
[28] M.F. Serra, M.S. Conconi, G. Suarez, E.F. Aglietti, and N.M. Rendtorff, Volcanic ash as flux in clay based triaxial ceramic materials, effect of the firing temperature in phases and mechanical properties, *Ceram. Int.*, 41(2015), No. 5, p. 6169.
[29] S. Vichaphund, K. Somton, T. Wonglom, M. Rodchom, and D. Atong, Utilization of basalt fibers as a raw material for clay ceramic production, *Ceram. Silik.*, (2016), p. 72.
[30] International Organization for Standardization, ISO 13006: *Ceramic Tiles—Definitions, Classification, Characteristics and Marking*, International Organization for Standardization, Geneva, 1998.
[31] R. Ji, Z.T. Zhang, C. Yan, M.G. Zhu, and Z.M. Li, Preparation of novel ceramic tiles with high $Al_2O_3$ content derived from coal fly ash, *Constr. Build. Mater.*, 114(2016), p. 888.
[32] A. Zimmer and C.P. Bergmann, Fly ash of mineral coal as ceramic tiles raw material, *Waste Manage.*, 27(2007), No. 1, p. 59.
[33] S.J. Ke, Y.M. Wang, Z.D. Pan, C.Y. Ning, and S.L. Zheng, Recycling of polished tile waste as a main raw material in porcelain tiles, *J. Clean. Prod.*, 115(2016), p. 238.
[34] T.K. Mukhopadhyay, S. Ghosh, S. Ghatak, and H.S. Maiti, Effect of pyrophyllite on vitrification and on physical properties of triaxial porcelain, *Ceram. Int.*, 32(2006), No. 8, p. 871.
[35] Y. Iqbal and W.E. Lee, Microstructural evolution in triaxial porcelain, *J. Am. Ceram. Soc.*, 83(2000), No. 12, p. 3121.
[36] Y.M. Park, T.Y. Yang, S.Y. Yoon, R. Stevens, and H.C. Park, Mullite whiskers derived from coal fly ash, *Mater. Sci. Eng. A*, 454-455(2007), p. 518.
[37] T.Y. Wang, S.H. Ma, X.H. Wang, T. Hong, and Y. Luo, A 100% high-aluminum fly ash-based high-density mullite ceramic with a triple microstructure: Preparation and mechanical characterization, *Constr. Build. Mater.*, 239(2020), art. No. 117761.
[38] R.F. Zhang, J.J. Feng, X.D. Cheng, L.L. Gong, Y. Li, and H.P. Zhang, Porous thermal insulation materials derived from fly ash using a foaming and slip casting method, *Energy Build.*, 81(2014), p. 262.